Optics Letters

High-quality high-throughput silicon laser milling using a 1 kW sub-picosecond laser

Daniel Holder,[1,*] Rudolf Weber,[1] Christoph Röcker,[1] Gerhard Kunz,[2] David Bruneel,[3] Martin Delaigue,[4] Thomas Graf,[1] and Marwan Abdou Ahmed[1]

[1]Institut für Strahlwerkzeuge (IFSW), University of Stuttgart, Pfaffenwaldring 43, 70569 Stuttgart, Germany
[2]Robert Bosch GmbH, Robert Bosch Campus 1, 71272 Renningen, Germany
[3]Lasea, Rue des Chasseurs Ardennais 10, 4031 Angleur, Belgium
[4]Amplitude Systemes, 11, Avenue de Canteranne, 33600 Pessac, France
*Corresponding author: daniel.holder@ifsw.uni-stuttgart.de

Received 5 October 2020; revised 12 November 2020; accepted 7 December 2020; posted 10 December 2020 (Doc. ID 411412); published 14 January 2021

We report on high-quality high-throughput laser milling of silicon with a sub-ps laser delivering more than 1 kW of average laser power on the workpiece. In order to avoid heat accumulation effects, the processing strategy for high-quality laser milling was adapted to the available average power by using five-pulse bursts, a large beam diameter of 372 μm to limit the peak fluence per pulse to approximately 0.7 J/cm^2, and a high feed rate of 24 m/s. As a result, smooth surfaces with a low roughness of $S_a \leq 0.6$ μm were achieved up to the investigated milling depth of 313 μm while maintaining a high material removal rate of 230 mm^3/min.

https://doi.org/10.1364/OL.411412

Laser processing with ultrafast lasers is a significantly growing field that offers high flexibility for advanced materials processing [1]. Recently, laser milling of silicon has gained widespread attention for applications such as dry etching of micro-electro-mechanical systems (MEMS) [2] and manufacturing of optics for THz radiation [3,4]. Most applications require high surface quality with a low roughness of $S_a < 1$ μm and the absence of surface defects, e.g., to achieve low scattering and hence high transmission in optics for THz radiation [5].

The surface quality obtained from laser milling of silicon with ultrashort laser pulses depends on various processing parameters. The applied fluence defines the resulting surface morphology on silicon, which can range from wavelength-sized laser-induced periodic surface structures (LIPSS) for low fluences to several micrometer large cones [6,7] and holes [8] as well as nanoscale solidification cracks on the silicon surface [9] for high fluences with single pulses. For equal fluence, pulse bursts can lead to smoother surfaces without holes in comparison to single pulses [8]. The surface morphology is also affected by the ambient environment. For instance, the formation of sharp spikes can be reduced using vacuum, N_2 or He [6]. Another processing parameter affecting the resulting surface morphology is the feed rate. With decreasing feed rate, a transition from a smooth reflecting surface to a bumpy dark surface was observed for processed metal surfaces [10]. The bumpy surface at lower feed rates is caused by higher surface temperatures due to heat accumulation of consecutive pulses [10,11]. Multiple passes over the processing area increase the milled depth, but also result in a coarser surface morphology [7], which typically corresponds to higher surface roughness values [4,7,8,10].

In addition to high surface quality, a high ablation efficiency is desired in order to achieve the maximum throughput with the available laser power. For laser milling, the ablation efficiency is often defined as the energy-specific volume, and the throughput is defined as the material removal rate. As shown in [8,12], pulse bursts can significantly increase the energy-specific volume of laser milling of silicon. The maximum attainable efficiency increases with increasing number of pulses per burst; however, it is accompanied by an increase in the surface roughness [12]. A trade-off for high-quality and high-efficiency silicon laser milling is to use five to eight pulses in burst in combination with a fluence at or slightly below the optimum fluence of maximum energy-specific volume. A roughness of $S_a = 0.5$ μm and an energy-specific volume of $\Delta V_E = 4.1$ μm^3/μJ were achieved with a five-pulse burst and a peak fluence per pulse of 1.5 J/cm^2 as reported in [8]. According to [12], eight pulses per burst and a peak fluence of 0.7 J/cm^2 per pulse resulted in a similar roughness of $S_a = 0.6$ μm, but with a significantly higher energy-specific volume of $\Delta V_E = 4.9$ μm^3/μJ. However, the throughput was rather low, with material removal rates of $\Delta V_t = 0.52$ mm^3/min and $\Delta V_t = 0.23$ mm^3/min, due to the low average laser power of 2.1 W and 0.9 W, respectively. Higher material removal rates of up to $\Delta V_t = 20$ mm^3/min have been demonstrated for silicon laser milling with up to 50 W of average laser power, but without further characterizing the surface roughness [13]. In the past, the average laser power limited the achievable throughput of ultrafast laser processes. With the upscaling of ultrafast lasers to powers exceeding 1 kW, high throughput has been made possible in many applications [14], such as multi-pass cutting of carbon fiber-reinforced plastics (CFRP) [15], surface functionalization of steel [16], or single-pass cleaving of glass [17].

Here, we report on high-quality high-throughput laser milling of silicon with a sub-ps laser with more than 1 kW of average power, which—to the best of our knowledge—is the first demonstration of material processing with sub-ps laser pulses at this power level.

A home-built ultrafast laser emitting pulses at a wavelength of $\lambda = 1030$ nm with a pulse duration of $\tau < 600$ fs was used for the experiments and is presented in detail in [18]. The ultrafast laser delivered a maximum average power of $P = 1110$ W with a beam quality factor of $M^2 < 1.5$. The linearly polarized laser beam was guided into a processing station (Lasea, LS 5-1) for the material processing experiments. The focusing optic (Scanlab, varioSCAN$_{de}$ 40i) with a focal length of 580 mm was mounted to the galvanometer scanner (Scanlab, intelliSCAN$_{de}$ 30) used for beam deflection. The transmission of the optics within the processing station was measured to be 91%, which results in a maximum average power of $P = 1010$ W on the workpiece. The laser was operated at a repetition rate of $f_b = 500$ kHz, corresponding to a maximum available total burst energy of $E_b = 2020$ μJ. In all experiments presented here, the burst energy was divided evenly over five pulses within the burst (5 PPB). The temporal intraburst pulse distance was 22.7 ns. The focal diameter was measured to be $d_0 = 90 \pm 5$ μm with the technique presented in [19]. The maximum available feed rate was $v_s = 24$ m/s, limited by the dynamics of the galvanometer scanner.

The processed samples were single, side-polished, silicon wafers with a diameter of 100 ± 0.3 mm, a thickness of 1000 ± 20 μm, and a crystal orientation of ⟨100⟩. The ablation experiments were conducted in ambient air on the polished side by scanning squares of 5×5 mm^2 along parallel offset lines with the hatching distance d_h. The sky-writing mode of the galvanometer scanner was used to ensure a constant feed rate v_s during scanning of the squares, resulting in a constant offset d_h between the impact locations of the individual bursts even at high feed rates. Multiple scans over the same squares were used to increase the depth of the milled cavities. The processed areas were characterized by means of a three-dimensional (3D) laser scanning microscope (LSM; Keyence, VK-9710-K). The measured cavity depth d_c was used to calculate the immanent material removal rate

$$\Delta V_t = \frac{d_b \cdot d_h \cdot d_c \cdot f_b}{n_s}, \tag{1}$$

where d_b and d_h denote the offset of the impact locations of the bursts on the surface in and perpendicular to the feed direction, respectively, f_b denotes the repetition rate, and n_s denotes the number of scans over the processed area. The material removal rate represents the ablated material volume per unit of time and is typically used to evaluate the throughput of an ablation process, and definition (1) only holds as long as the offsets d_b and d_h are kept so small to ensure a uniform ablation depth. The energetic efficiency of the ablation process is defined by the ratio of the ablated volume and the irradiated energy and is obtained by

$$\Delta V_E = \frac{\Delta V_t}{P}, \tag{2}$$

where P denotes the average laser power.

In a first step, we confirmed the advantageousness of a five-pulse burst and low peak fluence per pulse of approximately $\Phi_0 = 0.7$ J/cm^2, which were found to be beneficial in laser milling of silicon with regard to ablation efficiency and surface roughness as reported in [8,12], also for the pulse duration and repetition rate of our experimental setup, which significantly differs from the ones in [8,12]. The focal position was set on the sample's surface, corresponding to a beam diameter on the surface of $d_0 = 90$ μm. The feed rate of $v_s = 10$ m/s and the hatching distance $d_h = 20$ μm led to a burst overlap on the surface of 78% in both directions. The surface structure obtained by processing with $n_s = 20$ as measured by scanning electron microscope (SEM, Jeol JSM-6490LV) is shown in Fig. 1.

The surface is partially covered with LIPSS and nanoparticles. The period of the LIPSS was measured to 1040 ± 40 nm, which is close to the wavelength $\lambda = 1030$ nm of the irradiating laser beam and consistent with observations made in [6]. The nanoparticles detected on the surface vary in diameter from approximately 90 nm to 900 nm. The used parameters were suitable to avoid the formation of surface damage such as nanocracks or melt droplets larger than 1 μm in diameter. The impression of the smooth surface shown in Fig. 1 was confirmed by the low surface roughness which was measured to be $S_a = 0.5$ μm. This value is in good agreement with the values published in [8,12]. The energy-specific volume was measured to $\Delta V_E = 3.1$ μm^3/μJ, which corresponds to a material removal rate of $\Delta V_t = 10.6$ mm^3/min at an average power of $P = 57$ W.

In a second step, the average laser power was increased from $P = 57$ W to $P = 950$ W, which leads to an increase of the burst energy from $E_b = 114$ μJ to $E_b = 1900$ μJ. By shifting the focus position of the laser beam 17 mm (corresponding to approximately four Rayleigh lengths) below the sample surface, the beam diameter on the sample surface was increased from $d_0 = 90$ μm to $d_0 = 372$ μm to maintain a moderate peak fluence of $\Phi_0 = 0.70$ J/cm^2 at the high burst energy of $E_b = 1900$ μJ. As the surface temperature of the sample determines the formed surface structure, the increased amount of heat at this increased average power requires an adapted feed rate, which was shown to be a critical parameter affecting the accumulated heat on the surface [10]. The influence of the feed rate on the resulting surface structure and roughness for laser milling of silicon at the high average power of $P = 950$ W is shown in Fig. 2. The number of scans n_s were adapted with respect to the feed rate v_s so that the incident number of pulses and hence the total incident laser energy per unit area remains constant for all investigated data points. With the large beam diameter of $d_0 = 372$ μm required to keep the fluence at the desired value, the roughness obtained at a feed rate of $v_s = 10$ m/s amounts to $S_a = 3.6$ μm which is significantly higher than the one obtained in the aforementioned experiments with $P = 57$ W. At this low feed rate,

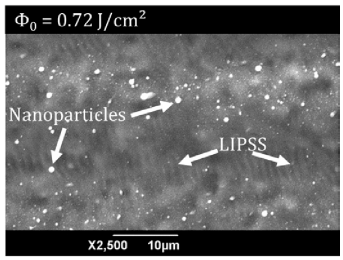

Fig. 1. SEM image of laser-milled surface. Process parameters: $\lambda = 1030$ nm, $P = 57$ W, $f_b = 500$ kHz, $E_b = 114$ μJ, PPB = 5, $d_0 = 90$ μm, $\Phi_0 = 0.72$ J/cm^2, $v_s = 10$ m/s, $d_h = 20$ μm, $n_s = 20$.

the elevated surface temperature caused by the high average power of 950 W led to the formation of melt, which resulted in a solidified melt film and nanoscale solidification cracks, as shown in Fig. 2(b). These surface defects were also observed in [9] for the ablation of craters with $\lambda = 355$ nm and $\tau = 20$ ps at a comparably higher peak fluence of $\Phi_0 = 40\ \mathrm{J/cm^2}$ and a much lower pulse repetition rate of $f_b = 50$ Hz. With increasing feed rate, the roughness decreases up to the lowest achieved value of $S_a = 0.4\ \mu$m at the maximum available feed rate of $v_s = 24$ m/s. The surface structure obtained with $v_s = 24$ m/s is shown in Fig. 2(c). The surface is covered with LIPSS and nanoparticles without larger surface damage. A major transition of the surface quality occurs in the feed rate range of about 14 m/s to 16 m/s, also referred to as the critical feed rate [10]. At 14 m/s and below, the roughness was $S_a > 1\ \mu$m, and the surface was mainly characterized by solidified melt films and nanocracks. As shown in Fig. 2(b), LIPSS are absent on the sample surface for a feed rate of $v_s = 10$ m/s due to the strong melt formation indicated by the solidified melt films. At 16 m/s and above, the roughness was $S_a < 1\ \mu$m, and the surface was covered only with LIPSS and nanoparticles. No significant changes in the diameter and distribution of nanoparticles were observed on the structured surfaces at the investigated feed rates.

The comparison of the results achieved at high power ($P = 950$ W) and $v_s = 24$ m/s [cf. Fig. 2(c)] with the results achieved at low power ($P = 57$ W) and $v_s = 10$ m/s (cf. Fig. 1) shows similar surface structure and roughness values with $S_a = 0.4\ \mu$m and $S_a = 0.5\ \mu$m, respectively. However, at a power of 950 W, the material removal rate is increased by a factor of 20 to $\Delta V_t = 216\ \mathrm{mm^3/min}$, which corresponds to an energy-specific volume of $\Delta V_E = 3.8\ \mu\mathrm{m^3/\mu J}$. The increased energy-specific volume at a similar peak fluence may be caused by defocusing the laser beam in order to increase the beam diameter on the sample surface. As the energy-specific volume is sensitive to the energy distribution on the irradiated surface, defocusing presumably changed the energy distribution of the defocused non-perfect Gaussian beam with the beam quality factor of $M^2 < 1.5$. An even higher energy-specific volume of $\Delta V_E = 9.6\ \mu\mathrm{m^3/\mu J}$ was recently reported in [20] using 1.76 GHz bursts with 100 pulses in the burst, but this caused an increased roughness of $S_a = 1.5\ \mu$m. The increased efficiency at the expense of quality with GHz bursts results primarily from a melt-assisted ablation process. For high surface quality with low roughness, a vaporization-dominated ablation process as demonstrated with our approach seems favorable.

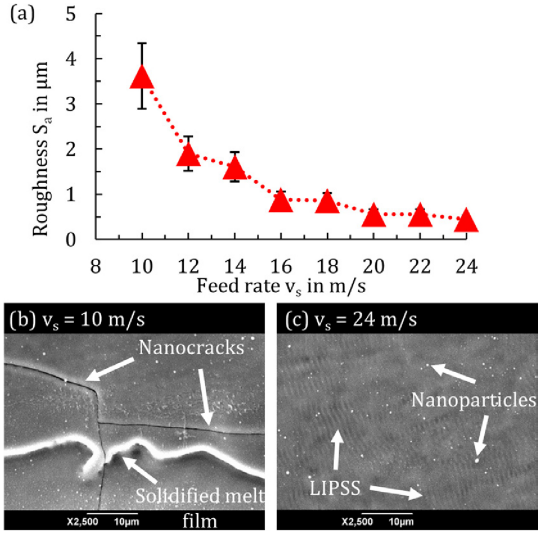

Fig. 2. (a) Mean roughness of the processed surfaces as a function of the feed rate with adapted number of scans to keep the total incident energy per unit area at a constant value of 19 J/mm^2. Error bars represent measurement uncertainties of ±20%. SEM images of corresponding surfaces at (b) $v_s = 10$ m/s and (c) $v_s = 24$ m/s. Process parameters: $\lambda = 1030$ nm, $P = 950$ W, $f_b = 500$ kHz, $E_b = 1900\ \mu$J, PPB = 5, $d_0 = 372\ \mu$m, $\Phi_0 = 0.70\ \mathrm{J/cm^2}$, $d_h = 50\ \mu$m.

The depth of the cavity milled with $v_s = 24$ m/s and $n_s = 24$ was measured to be $d_c = 72\ \mu$m. The low roughness and the avoidance of surface defects with diameters larger than 1 µm have to be maintained over a range of the cavity depth from a few microns up to several hundred microns in order to ensure surfaces that are suitable for the manufacturing of devices such as MEMS and THz optics. A simple method to adjust the cavity depth is the adaption of the number of scans n_s over the processed area. The resulting cavity depth and surface roughness using the parameters $P = 950$ W, $\Phi_0 = 0.70\ \mathrm{J/cm^2}$, and $v_s = 24$ m/s for a different number of scans are shown in Fig. 3.

Two distinct regimes can be identified with respect to the resulting roughness. The first regime with a roughness $S_a < 0.5\ \mu$m reaches a maximum of about 40 scans, which corresponds to a cavity depth of $d_c = 116\ \mu$m. The milled depth per scan in this first regime is approximately 3.0 µm. The second regime exhibits an increased roughness of $0.6\ \mu\mathrm{m} < S_a < 0.8\ \mu$m and ranges from 50 to 100 scans up to the maximum investigated cavity depth of $d_c = 313\ \mu$m. The milled depth per scan in the second regime is approximately 3.2 µm. A coarser surface structure and increased roughness with an increasing cavity depth was also observed for laser milling of silicon in [4,7]. However, in the present work, a low roughness $S_a < 0.8\ \mu$m and fine surface structure partially covered with LIPSS could be maintained up to the maximum milled depth of 313 µm [cf. Fig. 3(b)]. Both are required to avoid scattering and achieve maximum transmission when

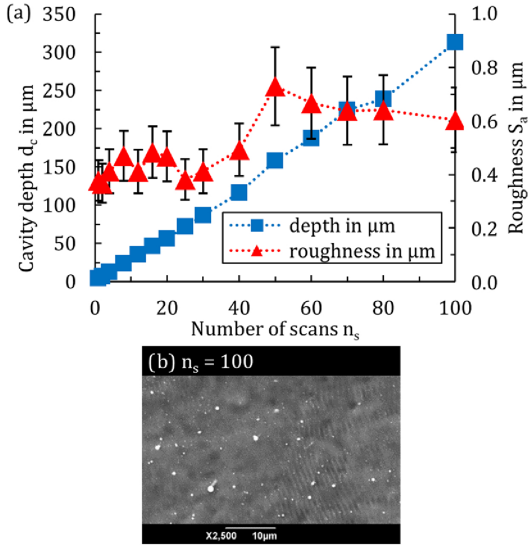

Fig. 3. Roughness and milled depth as a function of the number of scans. Error bars represent measurement uncertainties of ±20%. Process parameters: $\lambda = 1030$ nm, $P = 950$ W, $f_b = 500$ kHz, $E_b = 1900\ \mu$J, PPB = 5, $\Phi_0 = 0.70\ \mathrm{J/cm^2}$, $d_0 = 372\ \mu$m, $v_s = 24$ m/s, $d_h = 50\ \mu$m.

laser ablation is used for the manufacturing of optics for THz radiation.

Finally, we also demonstrated laser milling of a chamfer geometry by applying an average laser power in excess of 1 kW. To the best of our knowledge, this is the first demonstration of laser processing with sub-ps pulse durations and an average power of more than 1 kW. For this experiment, the available average power on the workpiece was increased to $P = 1010$ W by realignment of the laser system. As the beam diameter was kept constant, the resulting peak fluence on the workpiece was slightly increased to $\Phi_0 = 0.74\,\mathrm{J/cm^2}$. The chamfer geometry was milled by decreasing the width of one side of the initially squared-shaped scanning area after each scan by 50 μm, which corresponds to one parallel offset line with the hatching distance of $d_h = 50$ μm. An LSM measurement (Olympus, OLS4000) of the manufactured geometry is shown in Fig. 4.

The evaluation of the LSM measurements reveals low roughness values, with $S_a = 0.4$ μm in the upper area of the chamfer geometry (marked with I in Fig. 4) and $S_a = 0.6$ μm in the lower area of the chamfer geometry (marked with II in Fig. 4). The surface is again covered with LIPSS and nanoparticles (not shown here). This is consistent with the results obtained for laser milling of the flat surfaces shown in Fig. 3. Furthermore, the flatness of the tilted surface was investigated by calculation of the peak-to-valley height after filtering the LSM measurement with a cutoff wavelength of 250 μm. The tilted surface is smooth with a low peak-to-valley height of 5.7 μm over the large area of 3.5 × 3.5 $\mathrm{mm^2}$. Although the ablated depth per scan is about 3 μm, no steps were detected along the offset parallel processed lines.

The energy-specific volume of $\Delta V_E = 3.8\,\mu\mathrm{m^3/\mu J}$ during laser milling with $P = 1010$ W corresponds to a high material removal rate of $\Delta V_t = 230\,\mathrm{mm^3/min}$. To the best of our knowledge, this is the highest material removal rate reported so far for laser milling of silicon with ultrafast lasers, while at the same time achieving high surface quality with $S_a \leq 0.6$ μm and no surface defects with diameters exceeding 1 μm. In comparison to previously reported results for laser milling of silicon achieving low surface roughness, this is a 740 times greater removal rate than that reported in [12] and a 443 times greater material removal rate than that reported in [8]. Hence, the presented results show that high-power ultrafast lasers in combination with appropriate processing strategies such as bursts, low peak fluence, and high feed rates can significantly enhance the throughput of silicon laser milling while maintaining high surface quality. If small feature sizes are required that cannot be processed with a defocused laser beam, other techniques like beam shaping and beam splitting may be applied to distribute the pulse energy and effectively reduce the peak fluence on the workpiece.

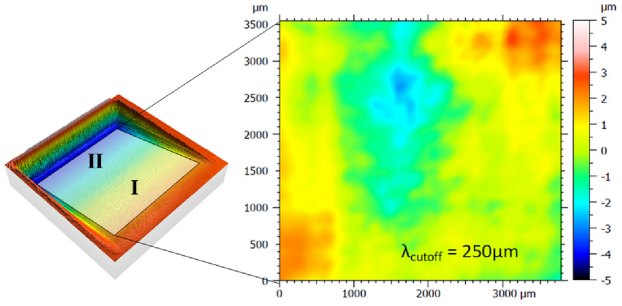

Fig. 4. LSM measurement of a chamfer milled on the surface of a silicon wafer. Process parameters: $\lambda = 1030$ nm, $P = 1010$ W, $f_b = 500$ kHz, $E_b = 2020$ μJ, PPB = 5, $\Phi_0 = 0.74\,\mathrm{J/cm^2}$, $d_0 = 372$ μm, $v_s = 24$ m/s, $d_h = 50$ μm. n_s was adapted for each scanning vector, up to 100 scans.

In conclusion, we demonstrated high-quality high-throughput silicon laser milling with an ultrafast laser delivering an average power of 1 kW which—to the best of our knowledge—is the first demonstration of material processing with sub-ps laser pulses at this elevated power level. To achieve this, a high-power ultrafast laser in combination with adapted processing strategies were used. A low surface roughness $S_a \leq 0.6$ μm and a smooth surface structure with LIPSS and nanoparticles were obtained at high average power by using pulse bursts, low peak fluences, and high feed rates. Furthermore, a low roughness was maintained up to the maximum investigated milling depth of 313 μm. The energy-specific volume was measured to be $\Delta V_E = 3.8\,\mu\mathrm{m^3/\mu J}$ at 1010 W on the workpiece, which corresponds to a material removal rate of $\Delta V_t = 230\,\mathrm{mm^3/min}$. Hence, high-power ultrafast lasers in combination with the appropriate processing strategies can significantly enhance the throughput while maintaining high surface quality.

Funding. H2020 Industrial Leadership (687880).

Disclosures. The authors declare no conflicts of interest.

REFERENCES

1. K. Sugioka and Y. Cheng, Light Sci. Appl. **3**, e149 (2014).
2. M. C. Gower, Proc. SPIE **4559**, 53 (2001).
3. L. Minkevičius, S. Indrišiūnas, R. Šniaukas, B. Voisiat, V. Janonis, V. Tamošiūnas, I. Kašalynas, G. Račiukaitis, and G. Valušis, Opt. Lett. **42**, 1875 (2017).
4. T. V. Kononenko, B. A. Knyazev, D. N. Sovyk, V. S. Pavelyev, M. S. Komlenok, G. A. Komandin, and V. I. Konov, Opt. Laser Technol. **123**, 105953 (2020).
5. S. Indrisiunas, E. Svirplys, H. Richter, A. Urbanowicz, G. Raciukaitis, T. Hagelschuer, H.-W. Hubers, and I. Kasalynas, IEEE Trans. Terahertz Sci. Technol. **9**, 581 (2019).
6. J. Bonse, S. Baudach, J. Krüger, W. Kautek, and M. Lenzner, Appl. Phys. A **74**, 19 (2002).
7. S. Lee, D. Yang, and S. Nikumb, Appl. Surf. Sci. **254**, 2996 (2008).
8. D. Metzner, P. Lickschat, and S. Weißmantel, Appl. Phys. A **125**, 172 (2019).
9. W. J. Keller, N. Shen, A. M. Rubenchik, S. Ly, R. Negres, R. N. Raman, J.-H. Yoo, G. Guss, J. S. Stolken, M. J. Matthews, and J. D. Bude, J. Appl. Phys. **125**, 85103 (2019).
10. F. Bauer, A. Michalowski, T. Kiedrowski, and S. Nolte, Opt. Express **23**, 1035 (2015).
11. R. Weber, T. Graf, P. Berger, V. Onuseit, M. Wiedenmann, C. Freitag, and A. Feuer, Opt. Express **22**, 11312 (2014).
12. B. Neuenschwander, B. Jaeggi, D. J. Foerster, T. Kramer, and S. Remund, J. Laser Appl. **31**, 22203 (2019).
13. R. Knappe, H. Haloui, A. Seifert, A. Weis, and A. Nebel, Proc. SPIE **7585**, 75850H (2010).
14. C. J. Saraceno, D. Sutter, T. Metzger, and M. A. Ahmed, J. Eur. Opt. Soc. **15**, 4169 (2019).
15. C. Freitag, M. Wiedenmann, J.-P. Negel, A. Loescher, V. Onuseit, R. Weber, M. Abdou Ahmed, and T. Graf, Appl. Phys. A **119**, 1237 (2015).
16. S. Faas, U. Bielke, R. Weber, and T. Graf, Sci. Rep. **9**, 1933 (2019).
17. T. Dietz, M. Jenne, D. Bauer, M. Scharun, D. Sutter, and A. Killi, Opt. Express **28**, 11415 (2020).
18. C. Röcker, A. Loescher, M. Delaigue, C. Hönninger, E. Mottay, T. Graf, and M. Abdou Ahmed, in *OSA Laser Congress* (Optical Society of America, 2019), pp. 1–2.
19. J. M. Liu, Opt. Lett. **7**, 196 (1982).
20. G. Bonamis, E. Audouard, C. Hönninger, J. Lopez, K. Mishchik, E. Mottay, and I. Manek-Hönninger, Opt. Express **28**, 27702 (2020).